Near-Infrared Emitting $CuInSe_2$/$CuInS_2$ Dot Core/Rod Shell Heteronanorods by Sequential Cation Exchange

Ward van der Stam,[†] Eva Bladt,[‡] Freddy T. Rabouw,[†] Sara Bals,[‡] and Celso de Mello Donega*[,†]

[†]Debye Institute for Nanomaterials Science, Utrecht University, P.O. Box 80000, 3508 TA Utrecht, The Netherlands and [‡]Electron Microscopy for Materials Science (EMAT), University of Antwerp, Groenenborgerlaan 171, B-2020 Antwerp, Belgium

ABSTRACT The direct synthesis of heteronanocrystals (HNCs) combining different ternary semiconductors is challenging and has not yet been successful. Here, we report a sequential topotactic cation exchange (CE) pathway that yields $CuInSe_2$/$CuInS_2$ dot core/rod shell nanorods with near-infrared luminescence. In our approach, the Cu^+ extraction rate is coupled to the In^{3+} incorporation rate by the use of a stoichiometric trioctylphosphine-$InCl_3$ complex, which fulfills the roles of both In-source and Cu-extracting agent. In this way, Cu^+ ions can be extracted by trioctylphosphine ligands only when the In—P bond is broken. This results in readily available In^{3+} ions at the same surface site from which the Cu^+ is extracted, making the process a direct place exchange reaction and shifting the overall energy balance in favor of the CE. Consequently, controlled cation exchange can occur even in large and anisotropic heterostructured nanocrystals with preservation of the size, shape, and heterostructuring of the template NCs into the product NCs. The cation exchange is self-limited, stopping when the ternary core/shell $CuInSe_2$/$CuInS_2$ composition is reached. The method is very versatile, successfully yielding a variety of luminescent $CuInX_2$ (X = S, Se, and Te) quantum dots, nanorods, and HNCs, by using Cd-chalcogenide NCs and HNCs as templates. The approach reported here thus opens up routes toward materials with unprecedented properties, which would otherwise remain inaccessible.

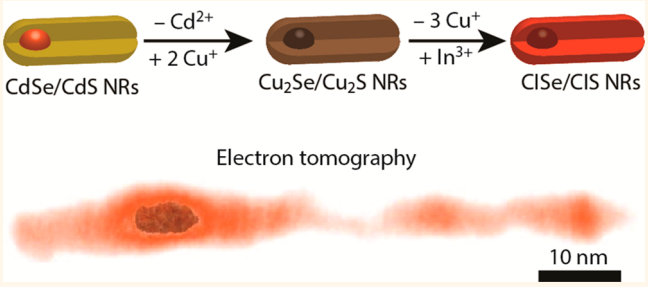

KEYWORDS: cation exchange · heteronanocrystals · quantum dots · nanorods · copper indium chalcogenide

The unique size- and shape-dependent properties of colloidal semiconductor nanocrystals (NCs), combined with their easy solution processability, have turned them into promising materials for a variety of technologies.[1] Colloidal NCs consisting of two (or more) different semiconductors (*i.e.*, heteronanocrystals, HNCs) offer even more possibilities regarding property engineering, since the carrier localization regime in these materials can be tailored by controlling the composition, size, and shape of each component and the architecture of the HNC.[1] Over the last decades, a remarkable degree of precision has been achieved in the synthesis of NCs and core/shell HNCs based on Cd- and Pb-chalcogenides (CdX and PbX, with X = S, Se, Te),[1−4] leading to materials with exceptional properties (*e.g.*, high quantum yields,[3] reduced blinking,[5,6] reduced threshold for lasing[7]). However, the large-scale deployment of these NCs is limited by the toxicity of Pb and Cd. This has stimulated a worldwide research effort on alternative materials that possess comparable properties and are less toxic.

Nanocrystals based on ternary I—III—VI semiconductors such as $CuInX_2$ are an attractive option, since their photoluminescence (PL) can be tuned from the visible to the near-infrared (NIR), which is relevant for applications such as light-emitting devices or biomedical imaging.[8−12] Moreover, they are also promising for applications in solar energy conversion (PV and photocatalysis).[9] However, the synthesis of ternary NCs is challenging, since multiple precursor reactivities must be simultaneously controlled. As a result, direct synthesis protocols for

* Address correspondence to c.demello-donega@uu.nl.

Received for review September 1, 2015 and accepted October 8, 2015.

Published online October 09, 2015
10.1021/acsnano.5b05496

colloidal $CuInX_2$ NCs are still largely underdeveloped[13−18] and do not offer the same degree of control available for Cd-based NCs. To date, it has not been possible to grow luminescent anisotropic ternary NCs or to combine two different $CuInX_2$ compounds into a single HNC by heteroepitaxial overgrowth. Here, we report a novel method that yields luminescent $CuInSe_2/CuInS_2$ (CISe/CIS) dot core/rod shell heteronanorods by applying sequential (Cu^+ for Cd^{2+} followed by self-limited partial In^{3+} for Cu^+) topotactic cation exchange (CE) reactions to template Cd-chalcogenide HNCs. The generality of our approach is demonstrated by converting a variety of Cd-chalcogenide (H)NCs into luminescent CuIn-chalcogenide (H)NCs, with preservation of the size, shape, and heteroarchitecture of the template NCs.

RESULTS AND DISCUSSION

Our approach is schematically depicted at the top of Figure 1 (see Experimental Methods for details), which also shows the optical spectra of a representative series of samples. The parent CdSe/CdS dot core/rod shell heteronanorods (NRs) show efficient PL at 2.07 eV and an absorption spectrum dominated by CdS transitions. After the Cu^+ for Cd^{2+} CE reaction the NRs become nonluminescent and exhibit an absorption spectrum typical of Cu-chalcogenides. After removal from the reaction mixture and washing, the Cu-based NRs are subjected to a partial In^{3+} for Cu^+ CE that yields NRs with PL in the NIR centered at 1.22 eV and an absorption spectrum that is consistent with CuIn-chalcogenide-based NCs (Figure 1). Sequential CE reactions (Cu^+ for Cd^{2+} followed by partial In^{3+} for Cu^+) were also performed on other CdSe/CdS dot core/rod shell NR samples and yielded similar results (Figure S1, Supporting Information, core diameters are in the range of

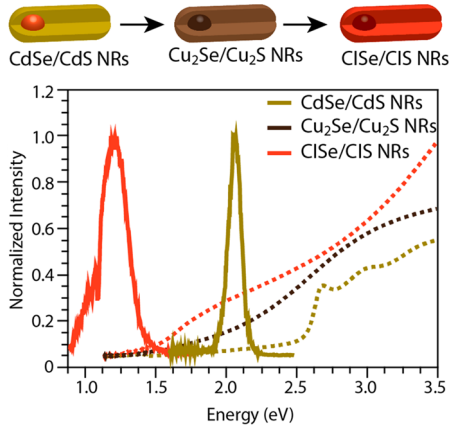

Figure 1. (Top) Schematic representation of the sequential cation exchange reaction, yielding ternary core/shell $CuInSe_2/CuInS_2$ (CISe/CIS) heteronanorods. (Bottom) Absorption (dashed lines) and photoluminescence (solid lines) spectra of the template CdSe/CdS NRs (orange lines), the intermediate Cu_2Se/Cu_2S NRs (brown lines), and the final product CISe/CIS NRs (red lines).

2.7, 3.1, and 3.2 nm and nanorod length/diameter are in the range of 51/5.2, 45/4.6, and 24/4.3 nm, for NRs emitting at 1.22, 1.19, and 1.17 eV, respectively).

Transmission electron microscopy (TEM) measurements show that the size and shape of the parent CdSe/CdS NRs are preserved in the product CISe/CIS NRs after the sequential CE reactions (Figure 2). Energy dispersive X-ray spectroscopy (EDS) measurements show a Cd:S ratio of 1:1 for the parent CdSe/CdS NRs, a Cu:S ratio of 2.1:1 for the intermediate Cu-based NRs, and a Cu:In:S ratio of 0.8:1.3:2 for the product CISe/CIS NRs (Figures S2 and S3, Supporting Information). Residual Cd^{2+} is observed in the intermediate Cu-based NRs (~2%), but is not detected in the product CISe/CIS NRs. These measurements indicate a successful sequential CE pathway toward CISe/CIS NRs. The product CISe/CIS NRs are accompanied by a byproduct of the CE reaction that was not completely removed by the washing-up procedure (see dark spots in Figure 2c and lighter particles in Figure S7a,b, Supporting Information). This byproduct is probably residual TOP-$InCl_3$ (TOP: trioctylphosphine; see Experimental Methods for details), since it consists only of In (*i.e.*, S and Cu peaks are not observed in the EDS measurements). Therefore, EDS spectra such as the one shown in Figure S2b (Supporting Information), which were collected over large areas containing both nanorods and byproduct, provide a reliable Cu:S ratio (1:2), but overestimate the In content. We corrected for this contribution by measuring EDS spectra on single NRs, which revealed a Cu:In:S ratio that is consistent with the $CuInS_2$ stoichiometry. EDS measurements were also carried out on small groups of isolated NRs, without the byproduct, yielding a Cu:In:S ratio of 0.8:1.3:2 (Figure S3, Supporting Information). We note that the Se signal of the core is not detected since the majority of the volume of the NRs consists of the metal sulfide compositions (CdS, Cu_2S, and CIS, respectively).

High-resolution (HR) high-angle annular dark field scanning TEM (HAADF-STEM) measurements also confirm the successful sequential cation exchange from parent CdSe/CdS dot core/rod shell NRs into product CISe/CIS dot core/rod shell NRs *via* intermediate Cu_2Se/Cu_2S dot core/rod shell NRs (Figure 2d−f). The HAADF-STEM investigation indicates that the parent CdSe/CdS core/shell NRs have the CdS wurtzite structure, since the fast Fourier transform (FFT) analysis of the HRTEM image (inset in Figure 2d) shows the characteristic {002} and {010} wurtzite CdS lattice planes (see also XRD pattern, Figure S4, Supporting Information). The thickness of the NRs varies from 9 to 15 atomic columns. Note that the majority of the volume of the NRs consists of CdS, and therefore the contribution of the CdSe core is not detected. FFT analysis of the HRTEM measurements shows that the product CISe/CIS NRs have the wurtzite $CuInS_2$ crystal structure (inset in Figure 2f; see also XRD pattern, Figure S4, Supporting

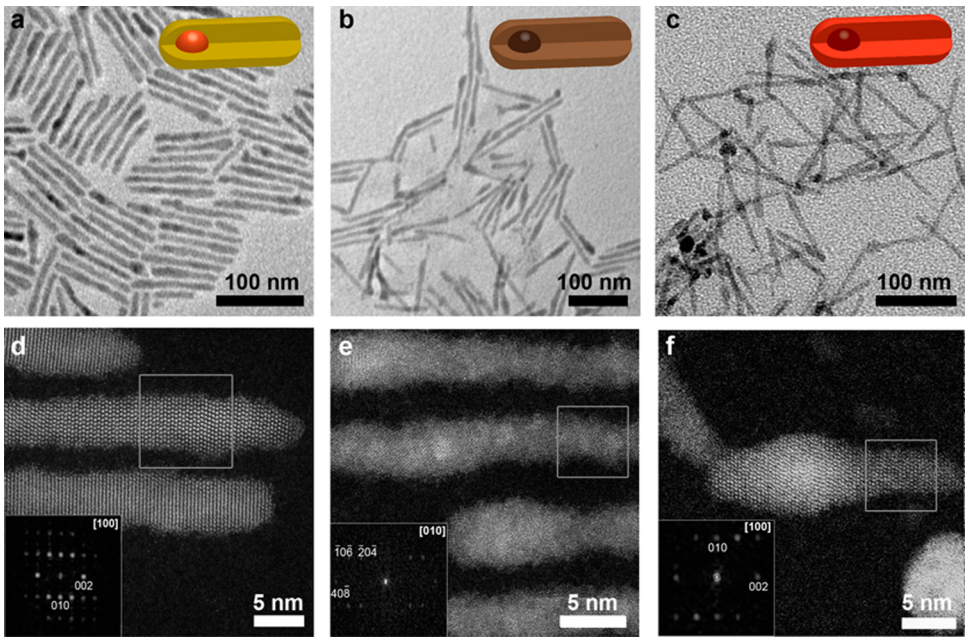

Figure 2. Transmission electron microscopy (a–c) and high-resolution HAADF-STEM (d–f) images of CdSe/CdS core/shell NRs (a, d), Cu_2Se/Cu_2S core/shell NRs (b, e), and $CuInSe_2/CuInS_2$ (CISe/CIS) core/shell NRs (c, f). The CISe/CIS NRs shown in c and f were obtained by sequential CE (Cu^+ for Cd^{2+} followed by partial In^{3+} for Cu^+) using the CdSe/CdS NRs shown in a and d as templates and the Cu_2Se/Cu_2S NRs shown in b and e as intermediates. The squares in panels d–f indicate regions where FFT analysis was performed. The corresponding FFT patterns show characteristic {010} and {002} wurtzite CdS reflections for CdSe/CdS core/shell NRs (inset panel d), characteristic chalcocite Cu_2S reflections for Cu_2Se/Cu_2S core/shell NRs (inset panel e), and characteristic wurtzite CIS reflections for CISe/CIS core/shell NRs (inset panel f). Additional HAADF-STEM images are provided in the Supporting Information (Figures S5–S7).

Information). From high-resolution HAADF-STEM imaging, we could determine that the resulting CISe/CIS NRs have a varying thickness of 8 to 14 atomic columns, consistent with the thickness of the template CdSe/CdS NRs. The position of the core was located by HAADF-STEM electron tomography (Figure 3). Since the intensity in HAADF-STEM images scales with the atomic number Z, this technique can distinguish between parts of the NRs containing Se ($Z_{Se} = 34$) and S ($Z_S = 16$). The electron tomography reconstruction shows that the cores are slightly elongated and that their shape is preserved in the product HNCs, showing that the anionic sublattice is not affected by the sequential CE reactions. We should note that the acquisition of several images at the same position of interest caused a lot of carbon contamination, due to the ligands covering the NRs. Therefore, the grids were baked at 120 °C for several hours in order to remove the organic ligands from the surface of the NRs. After this treatment, the organic contamination decreased, but also the shell of the CISe/CIS and Cu_2Se/Cu_2S NRs was slightly altered (Figure 3b,c).

Nanoscale cation exchange has emerged as a promising alternative for direct synthesis protocols, offering postsynthetic control over the composition and crystal structure, while preserving the size and shape of the parent NCs into the product NCs.[19] This allows access to NCs and HNCs otherwise not attainable.[19–32] Copper-chalcogenide NCs are often used as parent

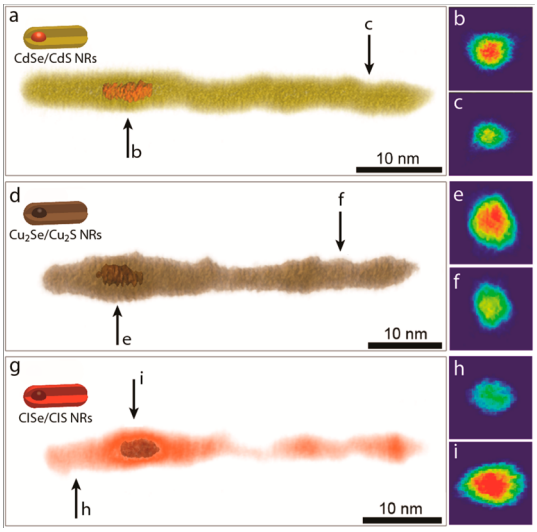

Figure 3. Visualizations of tomographic 3D reconstructions of (a) the template CdSe/CdS core/shell NRs (yellow, CdS; orange, CdSe), (d) the intermediate Cu_2Se/Cu_2S core/shell NRs (light brown, Cu_2S; dark brown, Cu_2Se), and (g) the final product $CuInSe_2/CuInS_2$ core/shell NRs (light red, $CuInS_2$; dark red, $CuInSe_2$). Orthoslices at positions marked with b and c for CdSe/CdS NRs, e and f for Cu_2Se/Cu_2S NRs, and h and i for $CuInSe_2/CuInS_2$ NRs show the position of the Se-containing cores, due to the difference in Z-contrast ($Z_{Se} = 34$ and $Z_S = 16$).

(template) NCs or intermediates in sequential CE reactions, because Cu^+ is easily exchanged by other cations.[19,21–27] For example, ZnSe/ZnS core/shell

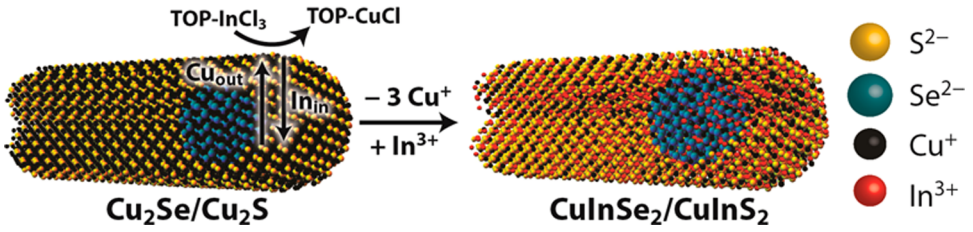

Figure 4. Schematic representation of the In^{3+} for Cu^{+} single-step CE reaction in Cu_2Se/Cu_2S core/shell heteronanorods. The Cu_{out} and In_{in} rates are now coupled, since Cu^{+} can be extracted by trioctylphosphine (TOP) only when In^{3+} is readily available for simultaneous incorporation.

NRs[21] and ultrathin nanoplatelets (NPLs)[27] have been obtained by sequential CE (Cu^{+} for Cd^{2+} followed by Zn^{2+} for Cu^{+}) in template CdSe/CdS core/shell NRs[21] and NPLs,[27] respectively, while wurtzite InP NPLs[25] were prepared by Cu^{+} for In^{3+} CE in template $Cu_{3-x}P$ NPLs. The exchangeability of Cu^{+} stems from its small charge and size, resulting in fast diffusion rates at the nanoscale, in combination with the availability of Cu-extracting ligands in solution.[19] Tri-*n*-octylphosphine is commonly used to extract Cu^{+} from NCs,[21,22,24−26] due to the strong affinity of the soft Lewis acid Cu^{+} (absolute hardness $\eta = 6.28$ eV)[33] and the soft base TOP ($\eta = 6$ eV).[33]

Recently, we demonstrated that CE reactions can be used to produce NCs of ternary semiconductors, by performing partial Cu^{+} for In^{3+} CE in $Cu_{2-x}S$ NCs, which resulted in luminescent wurtzite $CuInS_2$ NCs.[26] Interestingly, the CE reaction is self-limited in this case, stopping when the ternary $CuInS_2$ composition is reached. The self-limitation can be understood by considering the crystal structure of In_2S_3, which would require a reorganization of the anionic sublattice from hcp to fcc close-packing if the Cu^{+} for In^{3+} exchange were to reach completion forming In_2S_3.[26] This reorganization has a high activation barrier, since it requires the S−S distances of four out of every six anion layers to shift by over 58%.[26] We also found that the balance between the In^{3+} ingoing rate and the Cu^{+} outgoing rate is delicate and should be precisely balanced for a successful partial CE reaction to occur. When the out- and inward diffusion rates are not balanced, either the parent NCs dissolve or the CE reaction does not proceed at all. The imbalance between the in- and outgoing diffusion rates in $Cu_{2-x}S$ nanoplatelets subjected to In^{3+} for Cu^{+} CE has also been recently reported to result in hollow $CuInS_2$ nanoplatelets,[35] due to the nanoscale Kirkendall effect.[34,35]

In the present work, we apply an adaptation of our previous self-limited In^{3+} for Cu^{+} CE protocol[26] as the second step in a sequential topotactic CE reaction, through which template Cd-chalcogenide NCs and HNCs are first cation exchanged to Cu-chalcogenide NCs and HNCs and subsequently subjected to a partial In^{3+} for Cu^{+} CE. To improve the balance between the In^{3+} incorporation and the Cu^{+} extraction rates, we used a nearly stoichiometric TOP-$InCl_3$ complex (TOP/In ratio = 1.1), which fulfilled the roles of both In-source and Cu-extracting agent (Figure 4). In this way, the extraction and incorporation rates are strongly coupled, since Cu^{+} ions can be extracted by TOP ligands only when the In−P bond is broken. This results in readily available In^{3+} ions at the same surface site from which the Cu^{+} is extracted, making the process a direct place exchange reaction (similar to the case of Cd^{2+} for Zn^{2+} in ZnSe NCs)[20] and shifting the overall energy balance in favor of the CE, since In^{3+} ions are more stable in the NCs and Cu^{+} ions are more stable as TOP-Cu complexes in solution (bond dissociation energies in the gaseous state:[36] In−P, 198 kJ/mol; In−S, 289 kJ/mol; Cu−S, 285 kJ/mol). Cu−P dissociation energy is not available, but a strong interaction between Cu^{+} and TOP can be expected based on their similar chemical hardness η (*viz.*, 6.28 and 6 eV,[19,33] respectively). This approach is in contrast with previous works (including ours),[21,22,24−26] in which a large excess of TOP was used, resulting in fast extraction of Cu^{+} ions and decoupling of the in- and outward rates, since the Cu^{+} extraction and the In^{3+} incorporation then proceed by two separate chemical pathways.[26] As a result, the inward and outward rates can be influenced separately by choosing the right reaction parameters, but may also easily become imbalanced, especially in larger[26] and/or anisotropic NCs.[35] In the method developed in the present work, the imbalance is prevented, allowing controlled cation exchange to occur even in large and anisotropic heterostructured nanocrystals, such as the dot core/rod shell heteronanorods shown in Figures 2 and 3. In agreement with our previous work[26] and the discussion above, the In^{3+} for Cu^{+} CE reaction is self-limited, stopping when the ternary core/shell composition is reached, despite the fact that In^{3+} is in excess (both the Cu^{+} for Cd^{2+} and the In^{3+} for Cu^{+} CE reactions required a ~10:1 excess of the incoming cation with respect to the native cation).

It is interesting to note that our results imply that the inward and outward diffusion fluxes proceed at comparable rates through both the sulfide and selenide sublattices, since no evidence for a strong imbalance is observed. On the basis of the observations reported by Buhro and co-workers for In^{3+} for Cu^{+} CE in $Cu_{2-x}S$ nanoplatelets,[35] one could expect that either a hollow

center would develop (if Cu_{out} is faster than In_{in} in the selenide sublattice) or the shell would partially collapse (if Cu_{out} is faster than In_{in} in the sulfide sublattice), in the case where the rates are severely imbalanced. Our results provide no support for either of these limiting-case scenarios, indicating that the balance between the Cu_{out} and In_{in} rates is similar in both the selenide core and the sulfide shell (Figure 4). This is likely due to the similarity between the crystal structures and binding energies in the two materials (the lattice mismatch between wurtzite CISe and CIS is small, *viz.*, ~4%,[17,37] and the bond dissociation energies are 247 and 289 kJ/mol[36] for the In−Se and the In−S bonds, respectively, and 285 and 293 kJ/mol for the Cu−S and Cu−Se bonds,[36] respectively).

It should also be noticed that TOP coordinates not only to the soft Lewis acid Cu^+ but also to chalcogenides. In fact, TOP-chalcogen complexes with S, Se, and Te are widely used as chalcogen precursors in the synthesis of colloidal NCs of metal chalcogenides and are also important ligands to passivate surface states in these NCs.[1] Recently, TOP has also been shown to bind to chalcogenide ions in Cu chalcogenide NCs.[38] When nonstoichiometric Cu selenide NCs are exposed to a large excess of TOP, both Cu^+ and Se^{2-} ions are removed from the NCs,[38] increasing the concentration of vacancies and thereby accelerating the CE rates. However, in the present case, TOP is not in excess. In fact, all TOP available is complexed to $InCl_3$, and therefore, TOP is able to select only the preferred ions according to HSAB theory, *i.e.*, the softest acids, which, under the conditions prevalent in our experiments, will be the Cu^+ ions. Furthermore, we see no evidence for restructuring of the NCs after the second CE reaction. The effect of solvation of chalcogens by TOP on the CE rates is therefore negligible in the present case, due to the use of a (nearly) stoichiometric TOP-$InCl_3$ complex.

The PL excitation (PLE) spectrum of the CISe/CIS NRs closely matches the absorption spectrum (Figure 5a). This indicates that absorption anywhere in the CISe/CIS NR heterostructure, either in the CISe core or in the CIS rod shell, results in NIR emission. The situation is therefore analogous to the parent CdSe/CdS dot core/rod shell NRs, in the sense that the rod shell acts as an antenna that absorbs strongly and funnels excited charge carriers to the emissive core. The PL decay curve was fitted with a biexponential decay curve, with a fast component of 103 ns and a slow component of 1078 ns (Figure 5b). Such slow decay dynamics (with $\tau_1 \approx$ tens of ns and $\tau_2 \approx$ hundreds of ns) are typically encountered in $CuInX_2$ NCs.[9,39,40] Slow decay dynamics with a fast component of 100 ns and a slow component of 1 μs could be beneficial for the implementation of these CISe/CIS core/shell NRs into devices, since typically long carrier lifetimes are crucial for the effective extraction of charge carriers in photovoltaics[41] and are also beneficial for photocatalytic applications.[42]

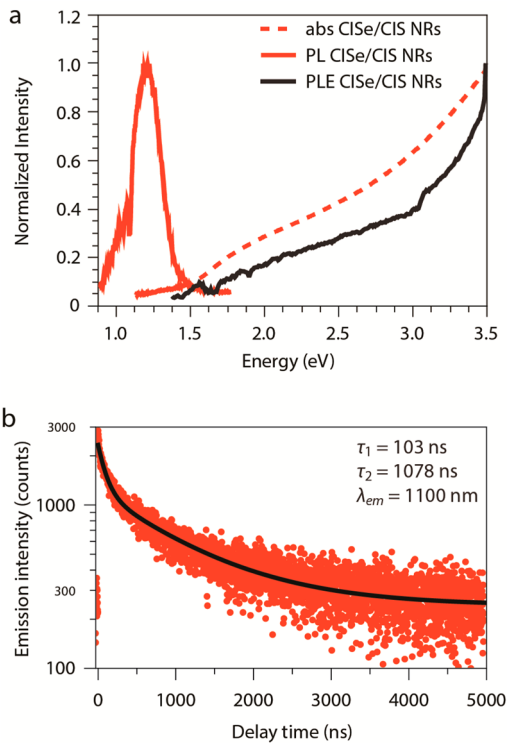

Figure 5. (a) Absorption (red dashed line), photoluminescence (PL, red full line), and PL excitation (PLE, black line) spectra of $CuInSe_2/CuInS_2$ core/shell NRs, obtained after sequential CE reactions. The PLE spectrum was acquired by setting the emission wavelength at the maximum of emission. (b) PL decay curve of $CuInSe_2/CuInS_2$ core/shell NRs obtained by sequential CE. Fitting a biexponential to the data (black curve) yields a fast component with τ_1 = 103 ns and a slow component with τ_2 = 1078 ns. The emission wavelength was set at 1100 nm.

Furthermore, our ternary CISe/CIS core/shell NRs provide the first system to study charge carrier dynamics at nanoscale heterointerfaces between two ternary I−III−VI semiconductors.

The carrier localization regime in semiconductor HNCs (*viz.*, type I, type I$^{1/2}$, or type II) can be tuned by controlling the composition, size, and shape of each component of the HNC.[1] This allows a number of properties (*e.g.*, exciton radiative lifetimes, exciton−phonon coupling strength, PL peak position and bandwidth, Stokes shift, Auger recombination rates, lasing threshold) to be tailored[1,5−7,43−45] and has therefore been extensively studied for HNCs based on Cd-chalcogenides and other II−VI semiconductors. In contrast, the impact of the energy offsets across nanoscale heterojunctions in HNCs based on ternary Cu-chalcogenides has not yet been addressed in detail and is likely to depend on the nature of the PL in these materials, which is nevertheless still under debate. Very often the PL of CIS NCs is assigned to a donor−acceptor pair recombination involving native point defects.[9,39,40] However, some studies ascribe it to the radiative recombination of quantized valence band hole states with trapped electrons,[46] while others

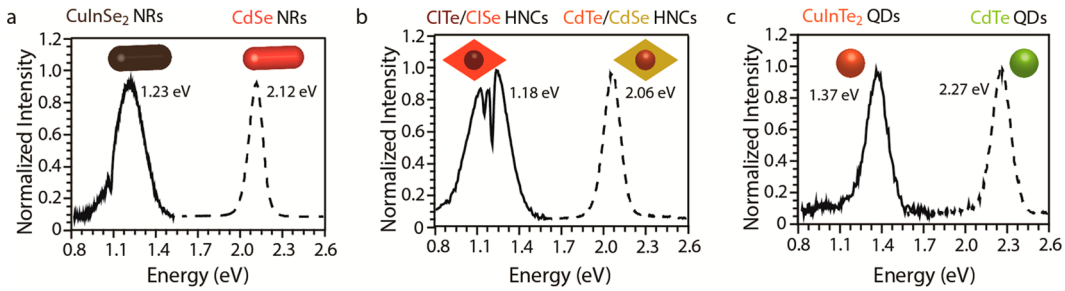

Figure 6. (a) PL spectra of parent CdSe NRs (dashed line) and of product $CuInSe_2$ NRs (solid line) obtained from the parent NCs by sequential CE (NR dimensions: 3 nm diameter, 4 nm long). (b) PL of parent core/shell CdTe/CdSe HNCs (dashed line) and of product $CuInTe_2/CuInSe_2$ HNCs (solid line) obtained from the parent HNCs by sequential CE (core diameter: 2.6 nm; HNC length: 4 nm). The fine structure observed in the PL peak of $CuInTe_2/CuInSe_2$ HNCs is due to absorption by the solvent used to disperse the HNCs (*viz.*, toluene). (c) PL of parent CdTe QDs (dashed line) and of product $CuInTe_2$ QDs (solid line) obtained from the parent NCs by sequential CE (QD diameter: 2.7 nm). The PL peak energies prior to and after the CE reactions are also given. PL and absorption spectra of parent spherical core/shell CdSe/CdS HNCs (dashed line), intermediate Cu_2Se/Cu_2S core/shell HNCs, and final product $CuInSe_2/CuInS_2$ core/shell HNCs (solid line), obtained by sequential CE reactions, are provided in the Supporting Information, Figure S8.

attribute it to recombination of quantized conduction band electron states with localized holes.[13] Recently, Efros and co-workers proposed that the PL of CIS QDs is analogous to that of the prototypical II–VI QDs and also originates from the 1S(e) → 1S(h) exciton transition.[47] This model precludes the involvement of trapped carriers and explains the intriguing characteristics of the PL of CIS NCs by the nature of the 1S(hole) fine-structure states.[47] The novel HNCs developed in the present work are likely to shed new light on the mechanisms behind the PL of CuIn chalcogenide NCs, thus contributing toward settling this long-standing debate. Such investigations are, however, beyond the scope of this paper.

To demonstrate the generality of our approach, we also carried out sequential CE reactions using spherical core/shell CdSe/CdS HNCs, prolate CdTe/CdSe HNCs, CdSe NRs, and different sizes of CdSe and CdTe quantum dots (QDs) as templates. In all these cases, the intermediate Cu-chalcogenide NCs did not show PL, whereas after self-limited partial In^{3+} for Cu^+ exchange, PL in the NIR was observed (Figure 6 and Figure S8, Supporting Information). It is interesting to notice that the NIR PL peak position is clearly correlated with the size, composition, and shape/architecture of the product NC or HNC [*e.g.*, the PL peak is at 1.37 eV for 2.7 nm diameter product CITe QDs and at 1.18 eV for product CITe/CISe core/shell HNCs (see Figure 6) and shifts from 1.22 to 1.17 eV upon increase of the CISe core diameter in product CISe/CIS dot core/rod shell NRs from 2.7 nm ± 0.4 nm to 3.2 nm ± 0.5 nm (see Figure S1, SI)]. This illustrates that the NIR PL of the product NCs (HNCs) can be tuned by a proper choice of the size, shape, composition, and heteroarchitecture of the template NCs (HNCs). Moreover, as discussed above, it may be possible to tailor the carrier localization regime in $CuInX_2$-based HNCs by controlling their composition, size, and heteroarchitecture. It should also be noted that topotactic Cu^+ for Cd^{2+} exchange in template Cd-chalcogenide NCs has already been successfully used by several groups to obtain a variety of Cu-chalcogenide colloidal nanostructures, such as ultrathin Cu_2Se/Cu_2S nanoplatelets,[27] $Cu_{2-x}S$ nanowires,[28] and $Cu_{2-x}Te$ QDs, NRs, and tetrapods.[29] This, in combination with the results reported in the present work, indicate that our approach is general and can be applied to any CdX (X = S, Se, and Te) 0D,[1] 1D (nanorods and tetrapods)[1] or 2D[48] NC or HNC (*e.g.*, CdSe/CdS dot core/rod shell heteronanorods[1,2] and heterotetrapods,[49] CdSe/CdS concentric core/shell QDs,[3] CdTe/CdSe core/shell heteronanorods and heteromultipods,[43,44] (Cd,Zn)Te/CdSe heteronanowires[50]), yielding size-, shape-, and composition-controlled ternary $CuInX_2$ NCs and HNCs that cannot be fabricated by direct synthesis methods.

CONCLUSIONS

In conclusion, we have shown successful sequential topotactic cation exchange (Cu^+ for Cd^{2+} followed by partial In^{3+} for Cu^+) from template Cd-chalcogenide core/shell HNCs into product CuIn-chalcogenide core/shell HNCs, *via* intermediate Cu-chalcogenide HNCs. The use of a stoichiometric TOP-$InCl_3$ complex efficiently couples the Cu^+ extraction and In^{3+} incorporation rates as well as the out- and inward diffusion rates, resulting in controlled cation exchange even in large and anisotropic heterostructured nanocrystals. This allowed us to synthesize for the first time colloidal $CuInSe_2/CuInS_2$ dot core/rod shell heteronanorods. The high-quality of these novel HNCs is attested by their near-infrared photoluminescence. The versatility of our method is demonstrated by successfully fabricating a variety of luminescent $CuInX_2$ (X = S, Se, and Te) quantum dots, nanorods, and HNCs, by using Cd-chalcogenide NCs and HNCs as templates. The approach reported here is thus general and allows the high precision and versatility achieved for the synthesis of Cd-chalcogenide NCs and HNCs to be

exploited to fabricate size-, shape-, and composition-controlled ternary $CuInX_2$ (hetero)nanocrystals, opening up routes toward materials with unprecedented properties, which would otherwise remain inaccessible.

EXPERIMENTAL METHODS

Materials. Cadmium oxide (CdO, 99.5%, trace metal basis), tetrakisacetonitrile copper(I)hexafluorophosphate ($[Cu(CH_3CN)_4]PF_6$), indium chloride ($InCl_3$, 99.999%), trioctylphosphine oxide (TOPO, tech., 90%), trioctylphosphine (TOP, 90%), octadecyl phosphonic acid (ODPA, 97%), 1-octadecene (ODE, tech., 90%), sulfur powder (S, 99.98%, trace metal basis), chloroform, anhydrous methanol, and anhydrous toluene were purchased from Sigma-Aldrich and used as delivered, except for TOPO and ODE, which were degassed prior to use by applying vacuum at 120 °C for 2 h. Selenium powder (Se, ~200 mesh, 99.999%) was bought from Brunschwig Chemie and used as supplied.

CdSe Nanocrystals. The NCs used as seeds were synthesized according to the method reported by Carbone *et al.*[2] A 0.060 g amount of CdO, 3.0 g of TOPO, and 0.290 g of ODPA were mixed in a 50 mL three-neck flask and heated to 150 °C under vacuum in a Schlenk line. After 2 h, the solution was heated to 330 °C under nitrogen until it became transparent. A 1.5 g portion of TOP was then injected, followed by heating to 370 °C and injection of TOP-Se (0.058 g of Se in 0.360 g of TOP). The NCs were allowed to grow for 7 min, after which the reaction was quenched by removal of the heating source. A 5 mL amount of toluene was injected when the temperature had dropped below 70 °C. In order to remove excess reactants, the CdSe NCs were washed three times by precipitation with methanol from a solution in toluene. The purified NCs were redispersed in toluene.

CdSe/CdS Dot Core/Rod Shell Nanorods. These NRs were synthesized using a seeded growth approach.[2] A 0.090 g amount of CdO, 3.0 g of TOPO, and 0.330 g of ODPA were mixed in a 100 mL three-neck flask and degassed at 150 °C under vacuum for 2 h in a Schlenk line. The reaction mixture was subsequently heated to 350 °C. When a transparent solution was obtained, 1.5 g of TOP was first injected, followed by the injection of a TOP−S solution (0.12 g of S in 1.5 g of TOP) and 200 μL of CdSe NC seeds in TOP (400 μM). After 12 min, the reaction was quenched by removal of the heating source and the NRs were washed by precipitation/redispersion with 5 mL of methanol and 5 mL of toluene.

Cu^+ for Cd^{2+} Cation Exchange. This CE was performed following the method reported by Li *et al.*[51] In a typical synthesis, 15 mg (0.04 mmol) of $[Cu(CH_3CN)_4]PF_6$ was dissolved into 2 mL of methanol and added to 4 mL of a CdSe/CdS NRs solution in toluene (~2×10^{-9} M). To ensure full exchange, a 10-fold excess of Cu^+ ions was used. The solution was stirred at room temperature for 5 min, after which the NRs were separated from the reaction solution by centrifuging at 3000 rpm for 5 min. Finally, the Cu_2Se/Cu_2S NRs were redispersed in 1 mL of toluene.

In^{3+} for Cu^+ Cation Exchange. This CE was performed using an adaptation of our recently reported method.[26] A 100 μL sample of a 2 M TOP-$InCl_3$ precursor in ODE (1 mmol of $InCl_3$ in 0.5 mL of TOP, diluted with 3 mL of ODE) was added to 0.5 mL of a diluted NC solution (10^{-9} M) in toluene at 100 °C. The solution was stirred for 4 h, after which the excess precursor was removed by precipitation with ~5 mL of methanol followed by redispersion in ~5 mL of toluene. This washing cycle was repeated twice.

Optical Spectroscopy. Samples for optical measurements were prepared by diluting the stock solution of washed NCs with anhydrous toluene under nitrogen and stored in sealed quartz cuvettes. Absorption spectra were measured on a double-beam PerkinElmer Lambda 16 UV/vis spectrometer. Photoluminescence and PL excitation spectra were recorded on an Edinburgh Instruments FLS920 spectrofluorimeter equipped with a 450 W xenon lamp as excitation source and double grating monochromators. PL decay curves were obtained by time-correlated single-photon counting on a liquid nitrogen cooled Hamamatsu R5509-72 photomultiplier tube. A pulsed diode laser (EPL-445 Edinburgh Instruments, 441 nm, 55 ps pulse width, 0.2 MHz repetition rate) was used as the excitation source.

X-ray Diffraction. XRD measurements were performed with a Bruker D2 Phaser, equipped with a Co Kα X-ray source (λ = 1.790 26 Å). Thin NC solid films for XRD were prepared by drop-casting a concentrated NC solution in chloroform on a Si wafer and evaporating the solvent.

Transmission Electron Microscopy. TEM images were acquired using a FEI Tecnai-10 microscope operating at 100 kV. Samples for TEM imaging were prepared by drop-casting a toluene solution of NCs onto a carbon-coated copper (400-mesh) TEM grid.

High-Resolution Transmission Electron Microscopy. HRTEM images were acquired on a Titan operating at 300 kV. The sample was drop-casted on an ultrathin grid to reduce the background signal from the carbon support and thereby improve the image quality.

Electron Tomography. Experiments were performed on a Tecnai G2 operating at 200 kV. Tilt series of 15 projection images were acquired in HAADF-STEM mode with an angular range from −70° to +70° and a tilt increment of 10°. Because the acquisition of several images at the same region of interest was causing an accumulation of contamination, the ultrathin grids were baked at 120 °C for several hours.

Energy Dispersive X-ray Spectroscopy. EDS measurements were performed on a FEI Tecnai G2 electron microscope operated at 200 kV, using a dedicated low-background holder and Cu-free Mo TEM grids. The EDS acquisition was carried out using a ChemiSTEM system and analyzed using the Bruker ESPRIT software. The following lines were used: S−K at 2.3 keV, In−L at 3.3 keV, and Cu−K at 8.0 keV. The In−L and Cu−K are well-resolved, but S−K partially overlaps with one of the Mo peaks at 2.4 keV. The software deconvoluted these two peaks in order to allow the quantification of the S content. To verify the elemental concentrations determined, EDS measurements were also performed on a FEI Tecnai-20F microscope operating at 200 kV, using a dedicated low-background holder and Cu-free Al TEM grids. The EDS signal is acquired with an EDAX Si(Li) detector and analyzed with the Tecnai Imaging and Analysis software, using the following lines: S−K at 2.3 keV, In−L at 3.3 keV, and Cu−K at 8.0 keV.

Conflict of Interest: The authors declare no competing financial interest.

Acknowledgment. The authors thank Gang Wang for XRD measurements and Eline Hutter for providing CdSe/CdS NRs. W.v.d.S. and C.d.M.D. acknowledge financial support from the division of Chemical Sciences (CW) of The Netherlands Organization for Scientific Research (NWO) under grant number ECHO.712.012.001. This work was supported by the European Research Council (ERC Starting Grant #335078 Colouratom). E.B. gratefully acknowledges financial support by the Flemish Fund for Scientific Research (FWO Vlaanderen).

Supporting Information Available: The Supporting Information is available free of charge on the ACS Publications website at DOI: 10.1021/acsnano.5b05496.

Optical spectra of $CuInSe_2/CuInS_2$ NRs of various dimensions, X-ray diffractograms, energy dispersive X-ray spectroscopy measurements, and additional HAADF-STEM images of CdSe/CdS, Cu_2Se/Cu_2S, and $CuInSe_2/CuInS_2$ core/shell heteronanorods, and photoluminescence and absorption spectra of parent spherical core/shell CdSe/CdS QDs, intermediate Cu_2Se/Cu_2S core/shell QDs, and final product $CuInSe_2/CuInS_2$ core/shell QDs (PDF)

REFERENCES AND NOTES

1. Donega, C. d. M. Synthesis and Properties of Colloidal Heteronanocrystals. *Chem. Soc. Rev.* **2011**, *40*, 1512–1546.
2. Carbone, L.; Nobile, C.; De Giorgi, M.; Della Sala, F.; Morello, G.; Pompa, P.; Hytch, M.; Snoeck, E.; Fiore, A.; Franchini, I. R.;

et al. Synthesis and Micrometer-Scale Assembly of Colloidal CdSe/CdS Nanorods Prepared by a Seeded Growth Approach. *Nano Lett.* **2007**, *7*, 2942–2950.
3. Chen, O.; Zhao, J.; Chauhan, V. P.; Cui, J.; Wong, C.; Harris, D. K.; Wei, H.; Han, H.-S.; Fukumura, D.; Jain, R. K.; *et al.* Compact High-Quality CdSe-CdS Core-Shell Nanocrystals with Narrow Emission Linewidths and Suppressed Blinking. *Nat. Mater.* **2013**, *12*, 445–451.
4. Tessier, M. D.; Mahler, B.; Nadal, B.; Heuclin, H.; Pedetti, S.; Dubertret, B. Spectroscopy of Colloidal Semiconductor Core/Shell Nanoplatelets with High Quantum Yield. *Nano Lett.* **2013**, *13*, 3321–3328.
5. Rabouw, F. T.; Lunnemann, P.; van Dijk-Moes, R. J. A; Frimmer, M.; Pietra, F.; Koenderink, A. F.; Vanmaekelbergh, D. Reduced Auger Recombination in Single CdSe/CdS Nanorods by One-Dimensional Electron Delocalization. *Nano Lett.* **2013**, *13*, 4884–4892.
6. Chen, Y.; Vela, J.; Htoon, H.; Casson, J. L.; Werder, D. J.; Bussian, D. A.; Klimov, V. I.; Hollingsworth, J. A. "Giant" Multishell CdSe Nanocrystal Quantum Dots with Suppressed Blinking. *J. Am. Chem. Soc.* **2008**, *130*, 5026–5027.
7. Klimov, V. I.; Ivanov, S. A.; Nanda, J.; Achermann, M.; Bezel, I.; McGuire, J. A.; Piryatinski, A. Single-Exciton Optical Gain in Semiconductor Nanocrystals. *Nature* **2007**, *447*, 441–446.
8. Kruszynska, M.; Borchert, H.; Parisi, J.; Kolny-Olesiak, J. Synthesis and Shape Control of $CuInS_2$ Nanoparticles. *J. Am. Chem. Soc.* **2010**, *132*, 15976–15986.
9. Kolny-Olesiak, J.; Weller, H. Synthesis and Application of Colloidal $CuInS_2$ Semiconductor Nanocrystals. *ACS Appl. Mater. Interfaces* **2013**, *5*, 12221–12237.
10. Yarema, O.; Bozyigit, D.; Rousseau, I.; Nowack, L.; Yarema, M.; Heiss, W.; Wood, V. Highly Luminescent, Size- and Shape-Tunable Copper Indium Selenide Based Colloidal Nanocrystals. *Chem. Mater.* **2013**, *25*, 3753–3757.
11. Panthani, M.; Stolle, C. J.; Reid, D. K.; Rhee, D. J.; Harvey, T. B.; Akhavan, V. A.; Yu, Y.; Korgel, B. A. $CuInSe_2$ Quantum Dot Solar Cells with High Open Circuit Voltage. *J. Phys. Chem. Lett.* **2013**, *4*, 2030–2034.
12. Zhong, H.; Zhou, Y.; Ye, M.; He, Y.; Ye, J.; He, C.; Yang, C.; Li, Y. Controlled Synthesis and Optical Properties of Colloidal Ternary Chalcogenide $CuInS_2$ Nanocrystals. *Chem. Mater.* **2008**, *20*, 6434–6443.
13. Li, L.; Pandey, A.; Werder, D. J.; Khanal, B. P.; Pietryga, J. M.; Klimov, V. I. Efficient Synthesis of Highly Luminescent Copper Indium Sulfide-Based Core/Shell Nanocrystals with Surprisingly Long-Lived Emission. *J. Am. Chem. Soc.* **2011**, *133*, 1176–1179.
14. Wang, X.; Swihart, M. T. Controlling the Size, Shape, Phase, Band Gap, and LSPR of $Cu_{2-X}S$ and Cu_XIn_YS Nanocrystals. *Chem. Mater.* **2015**, *27*, 1786–1791.
15. De Trizio, L.; Prato, M.; Genovese, A.; Casu, A.; Povia, M.; Simonutti, R.; Alcocer, M. J. P.; D'Andrea, C.; Tassone, F.; Manna, L. Strongly Fluorescent Quaternary Cu−In−Zn−S Nanocrystals Prepared from $Cu_{1-X}InS_2$ Nanocrystals by Partial Cation Exchange. *Chem. Mater.* **2012**, *24*, 2400–2406.
16. Stolle, C. J.; Schaller, R. D.; Korgel, B. A. Efficient Carrier Multiplication in Colloidal $CuInSe_2$ Nanocrystals. *J. Phys. Chem. Lett.* **2014**, *5*, 3169–3174.
17. Lu, X.; Zhuang, Z.; Peng, Q.; Li, Y. Controlled Synthesis of Wurtzite $CuInS_2$ Nanocrystals and Their Side-by-Side Nanorod Assemblies. *CrystEngComm* **2011**, *13*, 4039–4045.
18. Singh, A.; Coughlan, C.; Milliron, D. J.; Ryan, K. M. Solution Synthesis and Assembly of Wurtzite-Derived Cu−In−Zn−S Nanorods with Tunable Composition and Band Gap. *Chem. Mater.* **2015**, *27*, 1517–1523.
19. Beberwyck, B. J.; Surendranath, Y.; Alivisatos, A. P. Cation Exchange: A Versatile Tool for Nanomaterials Synthesis. *J. Phys. Chem. C* **2013**, *117*, 19759–19770.
20. Groeneveld, E.; Witteman, L.; Lefferts, M.; Ke, X.; Bals, S.; van Tendeloo, G.; Donega, C. d. M. Tailoring ZnSe-CdSe Colloidal Quantum Dots *via* Cation Exchange: From Core/Shell to Alloy Nanocrystals. *ACS Nano* **2013**, *7*, 7913–7930.
21. Li, H.; Brescia, R.; Krahne, R.; Bertoni, G.; Alcocer, M. J. P.; D'Andrea, C.; Scotognella, F.; Tassone, F.; Zanella, M.; De Giorgi, M.; *et al.* Blue-UV-Emitting ZnSe (dot)/ZnS (rod) Core/shell Nanocrystals Prepared from CdSe/CdS Nanocrystals by Sequential Cation Exchange. *ACS Nano* **2012**, *6*, 1637–1647.
22. van der Stam, W.; Gantapara, A. P.; Akkerman, Q. A.; Soligno, G.; Meeldijk, J. D.; van Roij, R.; Dijkstra, M.; Donega, C. d. M. Self-Assembly of Colloidal Hexagonal Bipyramid- and Bifrustum-Shaped ZnS Nanocrystals into Two-Dimensional Superstructures. *Nano Lett.* **2014**, *14*, 1032–1037.
23. Luther, J. M.; Zheng, H.; Sadtler, B.; Alivisatos, A. P. Synthesis of PbS Nanorods and Other Ionic Nanocrystals of Complex Morphology by Sequential Cation Exchange Reactions. *J. Am. Chem. Soc.* **2009**, *131*, 16851–16857.
24. van der Stam, W.; Akkerman, Q. A.; Ke, X.; van Huis, M. A.; Bals, S.; Donega, C. d. M. Solution-Processable Ultrathin Size- and Shape-Controlled Colloidal $Cu_{2-x}S$ Nanosheets. *Chem. Mater.* **2015**, *27*, 283–291.
25. De Trizio, L.; Gaspari, R.; Bertoni, G.; Kriegel, I.; Moretti, L.; Scotognella, F.; Maserati, L.; Zhang, Y.; Messina, G. C.; Prato, M.; *et al.* $Cu_{3-X}P$ Nanocrystals As a Material Platform for Near-Infrared Plasmonics and Cation Exchange Reactions. *Chem. Mater.* **2015**, *27*, 1120–1128.
26. van der Stam, W.; Berends, A. C.; Rabouw, F. T.; Willhammar, T.; Ke, X.; Meeldijk, J. D.; Bals, S.; Donega, C. d. M. Luminescent $CuInS_2$ Quantum Dots by Partial Cation Exchange in $Cu_{2-X}S$ Nanocrystals. *Chem. Mater.* **2015**, *27*, 621–628.
27. Bouet, C.; Laufer, D.; Mahler, B.; Nadal, B.; Heuclin, H.; Pedetti, S.; Patriarche, G.; Dubertret, B. Synthesis of Zinc and Lead Chalcogenide Core and Core/Shell Nanoplatelets Using Sequential Cation Exchange Reactions. *Chem. Mater.* **2014**, *26*, 3002–3008.
28. Zhang, D.; Wong, A. B.; Yu, Y.; Brittman, S.; Sun, J.; Fu, A.; Beberwyck, B.; Alivisatos, A. P.; Yang, P. Phase-Selective Cation-Exchange Chemistry in Sulfide Nanowire Systems. *J. Am. Chem. Soc.* **2014**, *136*, 17430–17433.
29. Kriegel, I.; Rodriguez-Fernandez, J.; Wisnet, A.; Zhang, H.; Waurisch, C.; Eychmuller, A.; Dubavik, A.; Govorov, A. O.; Feldman, J. Shedding Light on Vacancy-Doped Copper Chalcogenides: Shape-Controlled Synthesis, Optical Properties, and Modeling of Copper Telluride Nanocrystals with Near-Infrared Plasmon Resonances. *ACS Nano* **2013**, *7*, 4367–4377.
30. Beberwyck, B. J.; Alivisatos, A. P. Ion Exchange Synthesis of III-V Nanocrystals. *J. Am. Chem. Soc.* **2012**, *134*, 19977–19980.
31. Rivest, J. B.; Jain, P. K. Cation Exchange on the Nanoscale: an Emerging Technique for New Material Synthesis, Device Fabrication, and Chemical Sensing. *Chem. Soc. Rev.* **2013**, *42*, 89–96.
32. Gupta, S.; Kershaw, S. V.; Rogach, A. L. 25th Anniversary Article: Ion Exchange in Colloidal Nanocrystals. *Adv. Mater.* **2013**, *25*, 6923–6944.
33. Pearson, R. G. Hard and Soft Acids and Bases. *Inorg. Chem.* **1988**, *27*, 734–740.
34. Yin, Y.; Rioux, R. M.; Erdonmez, C. K.; Hughes, S.; Somorjai, G. A.; Alivisatos, A. P. Formation of Hollow Nanocrystals Through the Nanoscale Kirkendall Effect. *Science* **2004**, *304*, 711–714.
35. Mu, L.; Wang, F.; Sadtler, B.; Loomis, R. A.; Buhro, W. E. Influence of the Nanoscale Kirkendall Effect on the Morphology of Copper Indium Disulfide Nanoplatelets Synthesized by Ion Exchange. *ACS Nano* **2015**, *9*, 7419–7428.
36. Dean, J. A. *Lange's Handbook of Chemistry*, 15th ed.; McGraw-Hill, Inc.: New York, 1972; Section 4, Table 4.11, pp 4.44 and 4.47.
37. Norako, M. E.; Greaney, M. J.; Brutchey, R. L. Synthesis and Characterization of Wurtzite-Phase Copper Tin Selenide Nanocrystals. *J. Am. Chem. Soc.* **2012**, *134*, 23–26.
38. Lesnyak, V.; Brescia, R.; Messina, G. C.; Manna, L. Cu Vacancies Boost Cation Exchange Reactions in Copper Selenide Nanocrystals. *J. Am. Chem. Soc.* **2015**, *137*, 9315–9323.

39. Zhong, H.; Bai, Z.; Zou, B. Tuning the Luminescence Properties of Colloidal I−III−VI Semiconductor Nanocrystals for Optoelectronics and Biotechnology Applications. *J. Phys. Chem. Lett.* **2012**, *3*, 3167–3175.
40. Aldakov, D.; Lefrançois, A.; Reiss, P. Ternary and Quaternary Metal Chalcogenide Nanocrystals: Synthesis, Properties and Applications. *J. Mater. Chem. C* **2013**, *1*, 3756–3776.
41. McDonald, S. A.; Konstantatos, G.; Zhang, S.; Cyr, P. W.; Klem, E. J. D.; Levina, L.; Sargent, E. H. Solution-Processed PbS Quantum Dot Infrared Photodetectors and Photovoltaics. *Nat. Mater.* **2005**, *4*, 138–142.
42. Cowan, A. J.; Durrant, J. R. Long-Lived Charge Separated States in Nanostructured Semiconductor Photoelectrodes for the Production of Solar Fuels. *Chem. Soc. Rev.* **2013**, *42*, 2281–2293.
43. Donega, C. d. M. Formation of Nanoscale Spatially Indirect Excitons: Evolution of the Type-II Optical Character of CdTe/CdSe Heteronanocrystals. *Phys. Rev. B: Condens. Matter Mater. Phys.* **2010**, *81*, 165303.
44. Krumer, Z.; Pera, S. J.; van Dijk-Moes, R. J. A.; Zhao, Y.; de Brouwer, A. F. P.; Groeneveld, E.; van Sark, W. G. J. H. M.; Schropp, R. E. I.; Donega, C. d. M. Tackling Self-Absorption in Luminescent Solar Concentrators with Type-II Colloidal Quantum Dots. *Sol. Energy Mater. Sol. Cells* **2013**, *111*, 57–65.
45. Groeneveld, E.; Donega, C. d. M. Enhanced Exciton-Phonon Coupling in Colloidal Type-II CdTe-CdSe Heteronanocrystals. *J. Phys. Chem. C* **2012**, *116*, 16240–16250.
46. Kraatz, I. T.; Booth, M.; Whitaker, B. J.; Nix, M. G. D.; Critchley, K. Sub-Bandgap Emission and Intraband Defect-Related Excited-State Dynamics in Colloidal $CuInS_2$/ZnS Quantum Dots Revealed by Femtosecond Pump−Dump−Probe Spectroscopy. *J. Phys. Chem. C* **2014**, *118*, 24102–24109.
47. Shabaev, A.; Mehl, M. J.; Efros, Al. L. Energy Band Structure of $CuInS_2$ and Optical Spectra of $CuInS_2$ Nanocrystals. *Phys. Rev. B: Condens. Matter Mater. Phys.* **2015**, *92*, 035431.
48. Lhuillier, E.; Pedetti, S.; Ithurria, S.; Nadal, B.; Heuclin, H.; Dubertret, B. Two-Dimensional Colloidal Metal Chalcogenides Semiconductors: Synthesis, Spectroscopy, and Applications. *Acc. Chem. Res.* **2015**, *48*, 22–30.
49. Talapin, D. V.; Nelson, J. H.; Shevchenko, E. V.; Aloni, S.; Sadtler, B.; Alivisatos, A. P. Seeded Growth of Highly Luminescent CdSe/CdS Nanoheterostructures with Rod and Tetrapod Morphologies. *Nano Lett.* **2007**, *7*, 2951–2959.
50. Groeneveld, E.; van Berkum, S.; van Schooneveld, M. M.; Gloter, A.; Meeldijk, J. D.; van den Heuvel, D. J.; Gerritsen, H. C.; Donega, C. d. M. Highly Luminescent (Zn,Cd)Te/CdSe Colloidal Heteronanowires with Tunable Electron-Hole Overlap. *Nano Lett.* **2012**, *12*, 749–757.
51. Li, H.; Zanella, M.; Genovese, A.; Povia, M.; Falqui, A.; Giannini, C.; Manna, L. Sequential Cation Exchange in Nanocrystals: Preservation of Crystal Phase and Formation of Metastable Phases. *Nano Lett.* **2011**, *11*, 4964–4970.